Conference on Modelling Fluid Flow (CMFF'25)
The 19th International Conference on Fluid Flow Technologies
Budapest, Hungary, August 26 - August 29, 2025

A THROMBOSIS MODEL FOR BLOOD-CONTACTING MEDICAL DEVICES

Yuning Lin[2], Shuai Wang[3], Jianren Fan[1]

[1] Corresponding Author. State Key Laboratory of Clean Energy Utilization, Zhejiang University, 38 Zheda Road, Hangzhou 310027, China. Tel.: +0571-87951764, E-mail: fanjr@zju.edu.cn
[2] State Key Laboratory of Clean Energy Utilization, Zhejiang University. E-mail: linyuning@zju.edu.cn
[3] State Key Laboratory of Clean Energy Utilization, Zhejiang University. E-mail: wshuai2014@zju.edu.cn

ABSTRACT

Thrombus formation is crucial for blood-contacting medical devices. Current models focus on platelet activity or coagulation factors but overlook the interplay between these two processes, essential for accurate thrombus prediction. In this work, a thrombus generation model was developed, which couples platelet activity with the coagulation cascade. By utilizing the fibrin and thrombin, the product of the coagulation cascade, to regulate thrombus formation, the two processes are integrated. A reduced-order coagulation cascade model is employed, enabling the model to more closely align with human physiological processes while improving computational efficiency. The model's prediction of volume exhibited an error within 20% compared to experimental results and can effectively capture the evolutionary patterns of thrombus formation over time. This thrombus model is expected to be a reliable predictive tool for thrombus generation in blood-contacting medical devices.

Keywords: thrombus, blood-contacting medical devices, hemodynamics

NOMENCLATURE

C_i	$[mol/m^3]$	concentration of component i
D_i	$[N]$	diffusion coefficient of i
k_{apa}	$[/s]$	rate of platelet chemical activation
k_{spa}	$[/s]$	rate of shear-induced activation
k_{aps}	$[/s]$	activation rate due to other platelet-synthesized agonists
t	$[s]$	time
$\underline{v}$	$[m/s]$	absolute velocity vector of blood
$\underline{v_T}$	$[m/s]$	absolute velocity vector of thrombus
μ	$[Pa\cdot s]$	dynamic viscosity of blood
ϕ	[-]	thrombus volume fraction
τ	$[Pa]$	scalar shear stress
γ	$[/s]$	shear rate

1. INTRODUCTION

Blood-contacting medical devices have gained widespread clinical use in the management of cardiovascular and cardiopulmonary diseases. However, hemocompatibility-related complications, including bleeding and thrombosis, remain critical clinical challenges. For instance, left ventricular assist devices (LVADs) are an effective treatment for end-stage heart failure-related diseases. Nevertheless, device-induced thrombus may lead to stroke, neurological events, or compromised mechanical efficiency, ultimately necessitating device replacement [1]. Consequently, elucidating the mechanisms underlying thrombus formation in blood-contacting medical devices constitutes a critical research imperative to advance both device design optimization and clinical implementation.

Thrombus formation is a complex phenomenon governed by the coupled hemodynamic and physiological mechanisms, wherein platelets and biochemical mediators interact through cascade reactions, ultimately driving platelet activation, aggregation, adhesion, and stabilization. Given the incomplete understanding of device-induced thrombotic mechanisms and the inherent risks and difficulties of conducting clinical trials in patient populations, computational modeling of thrombus formation has emerged as an indispensable tool for bridging the fap between in vivo and in vitro experimentation [2]. For example, Fogelsen [3] pioneered simulations integrating platelet activation, agonists transport, and platelet bulk aggregation within continuum-model framework. The inherent complexity of modeling thrombus formation in blood-contacting devices - stemming from the coupled interactions of platelets with numerous biochemical species - necessitates a critical compromise between model fidelity and computational efficiency. Fogelsen and Guy [4] compared a microscale model of platelet aggregation with a continuum model of platelet aggregation and found that the continuum model took only 1% of the

computational time of the microscale model to obtain results similar to those of the microscale model. Based on the Fogelsen continuum model, Sorensen et al. [5] proposed a two-dimensional thrombus model for blood contact with medical devices that incorporates multiple biochemical agonists of platelets to more accurately describe the mechanisms of platelet activation. Goodman et al. [6] extended previous models [3, 5] by incorporating shear stress effects on platelet activation, enabling their model to achieve real-time spatial prediction of thrombus growth. Taylor et al. [7] modified the model of [3, 5] by proposing a simple computational network capable of doing verifiable macro-scale prediction of thrombus at the same spatial scale as cardiovascular devices on time scales ranging from minutes to hours. Wu et al. [8,9] further extended the former model [5] that accurately predicted thrombus generation under different flow conditions and biological environments and was the first to predict thrombus generation and growth in an axial blood pump, with results consistent with clinical observations. Blum et al. [10] developed an accelerated thrombosis model by simplifying a previous model [7] with a time step 10,000 times larger than the time step required by the pre-simplified model, which significantly improves the computational efficiency. Moreover, Li et al. [11–13] established a predictive model focusing on platelet dysfunction induced by supraphysiological shear stresses in blood-contacting devices. While these models focus on platelet activity, but as mentioned earlier, thrombus formation remains intrinsically regulated by coagulation cascades. Meanwhile, some studies have also started from the coagulation cascade reaction to predict thrombus generation and growth by modeling the kinetic process of the coagulation cascade [14–17]. Existing thrombus models typically focus on a single specific subprocess in thrombus formation, limiting their ability to comprehensively reveal the complex mechanisms of thrombus formation. This limitation arises from the trade-off between computational efficiency and the precision of capturing physiological processes. Specifically, thrombus models based on platelet activity often overlook the regulatory effects of the coagulation cascade on platelet behavior, while models based on the coagulation cascade, due to involving numerous reactants and complex reaction networks, result in excessively high computational costs, making efficient simulations challenging.

To address the limitations of previous research, this work proposes a coupled thrombosis model that integrates hemodynamics, platelet activity, and the coagulation cascade. The model regulates platelet activation, aggregation, adhesion, and stabilization through the intermediate and terminal products of the coagulation cascade. To improve computational efficiency, this study utilizes a reduced-order coagulation cascade model. Additionally, the model incorporates dynamic interactions between blood flow and thrombus formation, with particular consideration of shear stress effects in thrombus breakdown under hemodynamic conditions. This thrombus model was then applied to a backward-facing step geometry and validated in space and time against the experiments to assess the accuracy of the predictions of model.

2. METHODS

This work develops a mathematical model of thrombosis. The model couples the fluid governing equations and introduces convection-diffusion-reaction equations (CDR equations) to describe the transport of a range of biochemicals such as platelets and coagulation factors. Chemical activation and shear activation are considered for platelets, and platelet deposition is considered in terms of biochemical concentration aspects and flow aspects. A resistance term is added to the fluid governing equation to represent the obstruction of blood flow by thrombus.

2.1 Governing Equations of Blood Flow

The flow of blood was represented using a modified Navier–Stokes equations (N-S equations):

$$\nabla \cdot \underline{v} = 0 \tag{1}$$

$$\rho\left(\frac{d\underline{v}}{dx} + \underline{v}\cdot\nabla\underline{v}\right) = -\nabla p + \mu\nabla^2\underline{v} + \frac{C_2}{(1-\phi)} f(\phi)(\underline{v} - \underline{v}_T) \tag{2}$$

where ρ is the density of the blood, μ is the kinetic viscosity of the blood, $\underline{v}$ is the flow rate of the blood, and $\underline{v}_T$ is the speed of the thrombus. The source term $C_2 f(\phi)(\underline{v}-\underline{v}_T)/(1-\phi)$ is the resistance exerted by the thrombus to the fluid, where $f(\phi) = \phi\,(1+6.5\phi)$; ϕ is the thrombus volume fraction.

2.2 Biochemical Component Equations

The thrombus model contains two sub-models, the platelet activity model and the coagulation cascade model, which describes the process of platelet aggregation, adhesion, deposition on the surface of a blood-contacting device, which is modulated by the coagulation cascade reaction, and finally by the concentration of fibrin monomers leading to the formation of a stable thrombus. The platelet activity model incorporates a platelet-released agonist, adenosine diphosphate (ADP), three states of platelets: resting platelets (RP), activated platelets (AP), and bound platelets (BP), and residence time. The residence time (RT) is used to determine the flow stagnation and recirculation zones. The coagulation cascade model contains nine coagulation factors and heparin. Some coagulation factors promote thrombin production, while some coagulation factors consume already produced thrombin thereby slowing down the progress of the coagulation cascade reaction. As shown in Figure 1,

when blood contacts the foreign surface, factor XII adsorbs to the surface, and triggers the coagulation cascade response.

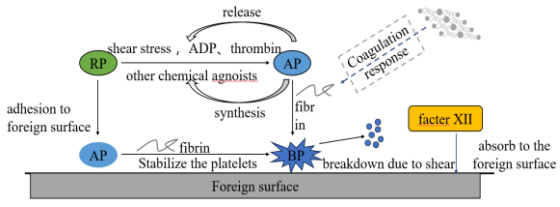

(a)

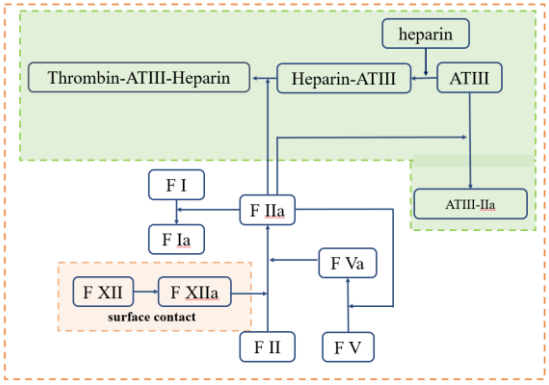

(b)

Figure 1. Schematic diagram of thrombus modeling mechanisms showing the role of the coagulation cascade in regulating platelet activity. (a) Platelet activity model. (b) Simplified coagulation cascade reaction with fibrin as the end product.

The transport phenomenon of biochemical substances is represented by the CDR equation:

$$\frac{\partial[C_i]}{\partial t}+\nabla\cdot\left(\underline{v}\cdot[C_i]\right)=\nabla\cdot\left(D_i\cdot\nabla[C_i]\right)+S_i \qquad (3)$$

where $[C_i]$ denotes the concentration of component i, D_i denotes the diffusion coefficient of i, and S_i is the source term of component i. The detailed diffusion coefficients and source terms are presented in [18].

The source term for platelet activation is defined as (Eq. (4)):

$$S_{AP}=k_{apa}\cdot RP+s_{spa}\cdot RP+k_{aps}\cdot RP \qquad (4)$$

where k_{apa} represents the rate of platelet chemical activation, k_{spa} denotes the rate of shear-induced activation, and k_{aps} refers to the activation rate due to other platelet-synthesized agonists.Since BP is not transported with blood, its governing equation is:

$$\frac{\partial BP}{\partial t}=S_{BP}-k_{tb}\phi \qquad (5)$$

where k_{tb} denotes the rate for thrombus breakdown, with a detailed definition provided in Table A1 in the appendices and [18].

RP directly attaches to the wall surface, transforming into AP, while FXII adhesion to the foreign surface. Both processes are governed by flux boundary conditions [5]. ADP is released when RP is converted to AP, and FXII adsorbed to the surface of the device is converted to FXIIa. Consequently, the boundary conditions for both processes are also expressed using flux boundary conditions. The boundary condition expressions are provided in Table A2 in the appendices.

2.3 Simulation Setup

The thrombus model is first validated in the backward-facing step (BFS) geometry, and the simulation results are quantitatively compared with the experimental data of Yang et al. [19]. The detail of the BFS geometry and mesh is shown in Figure 2. Mesh generation uses structural meshes. A boundary layer consists of 10 layers, and mesh refinement is applied in the BFS region. Given that the coagulation cascade in the model is initiated by contact activation, the numerical algorithm incorporates wall flux boundary conditions to implement this mechanism. Consequently, the size of the wall mesh will influence the accuracy of the model. To address this issue, three sets of grids with varying degrees of refinement were generated in the BFS region: 80% refined mesh, baseline mesh, and 120% refined mesh, in order to validate the accuracy of thrombus formation predictions. Based on the experimental setup, the inlet flow rate was set to 1.67×10^{-5} m³/s, the outlet was specified with a zero-pressure boundary condition, and all wall surfaces were considered as foreign surfaces. Since heparin was not used in the experiments, the initial concentration of heparin was set to 0, and γ_t was adjusted to 10 s^{-1}[20], while other settings remained unchanged. The initial conditions for the thrombus model are outlined in Table 1.

Table 1. Initial conditions for some biochemical species

species	unit	value
RP	PLT/m^3	1.85×10^{14}
AP	PLT/m^3	1%[RP]
XII	mol/m^3	9.36×10^{-8}
heparin	mol/m^3	1×10^{-4}

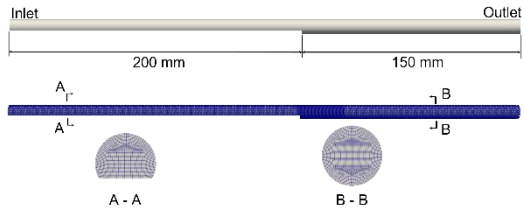

Figure 2. backward-facing step geometry

3. RESULT and DISCUSSION

As the coagulation cascade model is activated through the adsorption of FXII onto foreign surfaces, triggering the intrinsic coagulation cascade, the size of the boundary mesh is one of the key numerical factors in the thrombus model. To validate the mesh independence of the model, point A was selected in the BFS region, as shown in Figure 3(a). Figure 3(b) and Figure 3(c) present the temporal variation of concentrations of fibrin and AP at points A. The maximum deviations between the 80% refined, baseline, and 120% refined meshes were all below 3%, and as time progressed, the discrepancies among the three meshes progressively diminished and converged, ensuring the mesh independence of the thrombus model. Therefore, the baseline mesh, consisting of approximately 540,000 mesh elements, was chosen for the analysis.

Figure 4 shows the streamlines in the BFS region before thrombus formation. A recirculation zone is observed, with zero velocity at the corner after the sudden expansion and at the reattachment point downstream of the expansion, where the strain rate is less than 10 s^{-1}. Figure 5(a) presents a snapshot of the thrombus formed at t=20 s in the BFS region. Figures 5(b-e) illustrate the development of the thrombus and the corresponding velocity contours around the thrombus. The thrombus initially forms at the corner of the sudden expansion, with further thrombus formation occurring at the reattachment point downstream of the expansion. This is due to the low flow velocity and strain rate at both the step corner and reattachment point (Fig. 4), which promotes thrombus formation at these locations. This observation is consistent with the experimental and simulation results of Goodman et al. [6] and the simulations of Taylor et al. [7] However, this phenomenon was not observed in the experiments of Yang et al. [19], possibly due to the resolution limitations of MRI. Subsequently, the thrombus formed at the step corner propagates downstream, while the thrombus formed at the reattachment point propagates upstream, until the thrombi formed at both locations merge into a single thrombus. Additionally, both the thrombus growth and the corresponding velocity contours indicate that the thrombus formation alters its surrounding flow field.

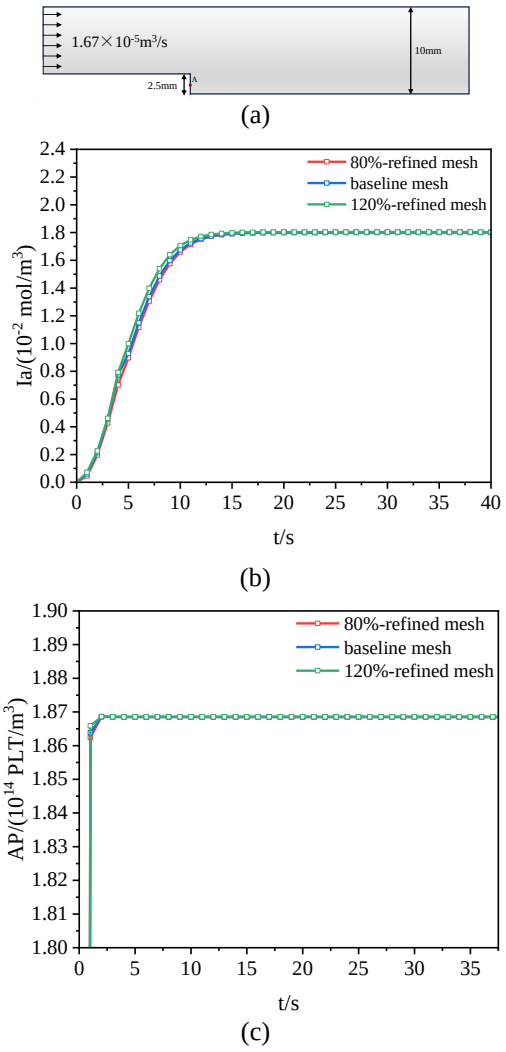

Figure 3. Mesh independence validation of the thrombus model. (a) Points A was selected for mesh independence validation, with coordinates A(0, -0.004, 0). Temporal variation of (b) fibrin and (c) AP concentrations at point A for the three grid

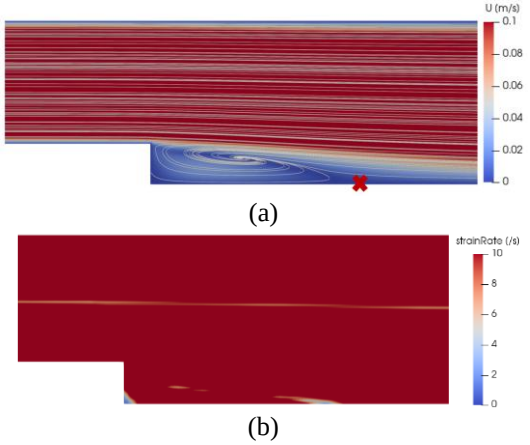

Figure 4. At t=1s, (a) streamline plot with a mark representing the reattachment point, (b) fluid strain rate.

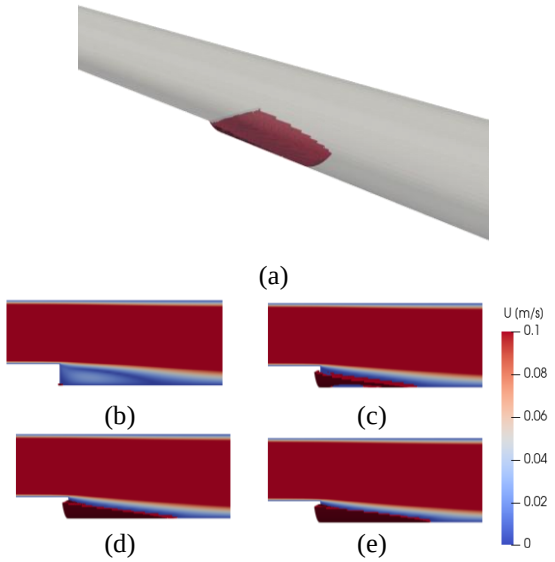

Figure 5. Simulated thrombus and flow field. (a) Simulated thrombus formed at t=20 s and streamline plot. (b-e) Simulated thrombus formed at t=2 s,6 s,10 s,14 s and velocity contours at the central cross-section.

The simulation results of the thrombus model in the BFS geometry are quantitatively compared with the experimental results of Yang et al. in both spatial and temporal domains, as shown in Figure 6. The time scale represented in Figure 6 is accelerated. Simulated results for thrombus volume, length, and height are in good agreement with the experimental data, demonstrating the model's capability to predict thrombus formation. Figure 6(a) compares the simulated thrombus volume with the experimental data. Thrombus formation begins at t=2 s, with the growth rate reaching its peak between t=3 s and t=7 s, after which the thrombus formation rate gradually slows. Figure 6(b) shows the comparison of the simulated thrombus length with the experimental results. Between t=2 s and t=6 s, the thrombus length increases rapidly. From t=6 s to t=8s, the growth rate of thrombus length significantly slows, and after t=8 s, the thrombus length hardly changes. Figure 6(c) illustrates the change in thrombus height over time, with the thrombus rapidly growing to nearly the height of the step before t=6 s, after which the thrombus height shows little further increase. Importantly, it is observed that during thrombus growth, the phenomenon of reattachment point drift occurs in the flow field. The numerical simulation framework is capable of effectively identifying this dynamic process. Notably, the consistency between the predicted thrombus distribution near the reattachment point and experimental results may be attributed to the model's ability to preset the reattachment point location, thereby ensuring a stable computational flow field and aligning simulation predictions with experimental observations.

Figure 7 illustrates the temporal evolution of concentration distributions for certain biochemical species. Figure 7(a) shows the distribution of AP concentration. Due to the strong platelet activation during the computational domain, the temporal variation in AP concentration is not significant. The concentration distribution of fibrin, as depicted in Figure 7(b), is influenced by a recirculation region downstream of the sudden expansion. Consequently, fibrin first accumulate at the corner of the sudden expansion and the reattachment point downstream, resulting in elevated concentrations. However, as the coagulation cascade progresses, the fibrin concentration becomes more uniform downstream. Notably, thrombus formation is influenced by both physiological factors and hemodynamic conditions. Over time, the fibrin concentration on the foreign surface tends to become consistent, but not all regions with high AP and fibrin concentrations develop into thrombi (Figure 7(c)). This is because platelet stabilization also depends on fluid shear stress. Only in low-shear regions can APs convert to BP, thereby forming a thrombus, as shown in Figure 8.

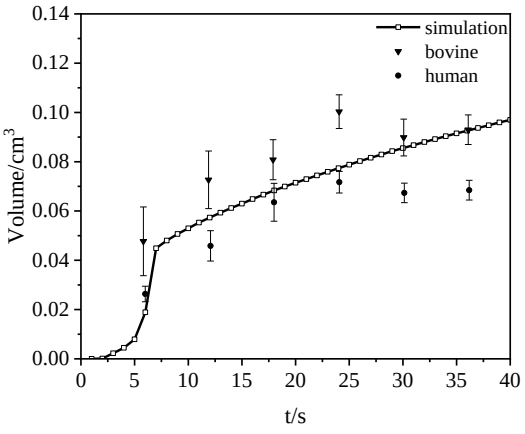

(a)

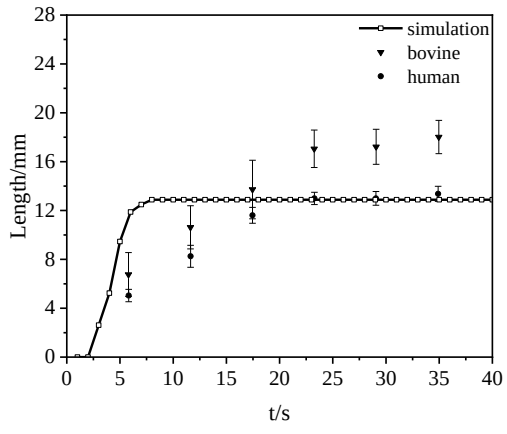

(b)

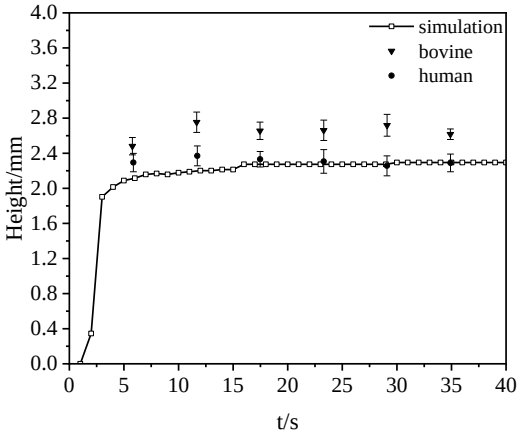

(c)

Figure 6. Quantitative comparison of the simulated thrombus with experimental data in both spatial and temporal domains. (a) Volume, (b) Length, (c) Height, with data obtained from Yang et al. [19].

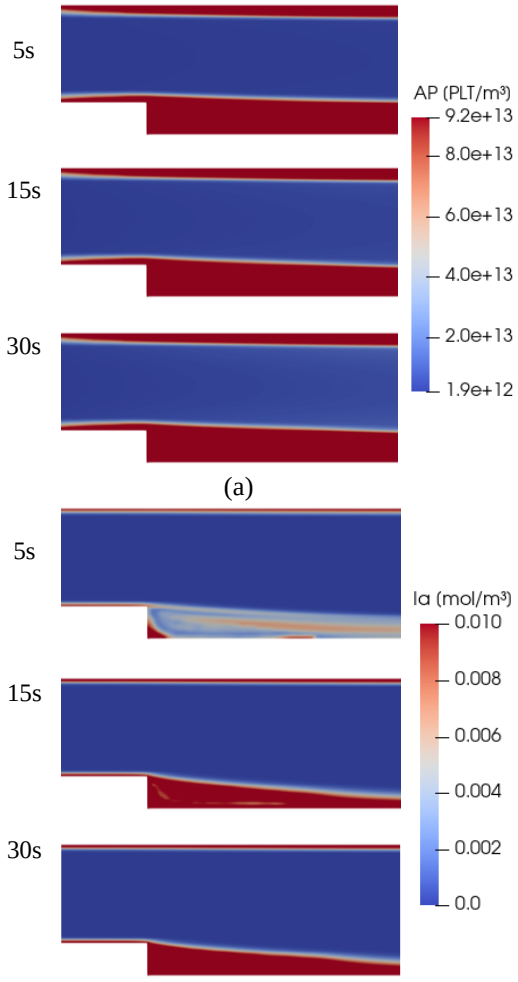

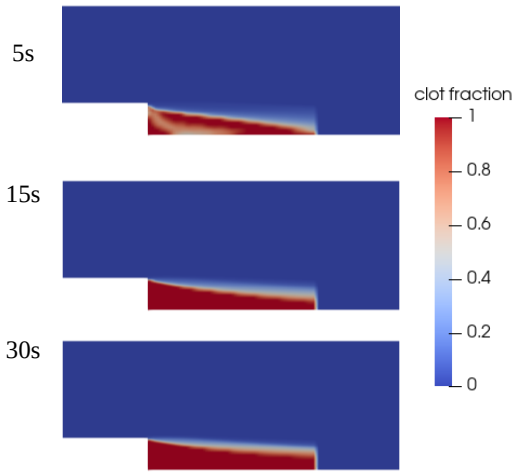

(c)

Figure 7. Concentration distribution of selected biochemicals and simulated thrombus volume fraction at t=5, 15 and 30s. (a) concentration ofAP. (b) concentration of fibin. (c) similated thrombus volume fraction.

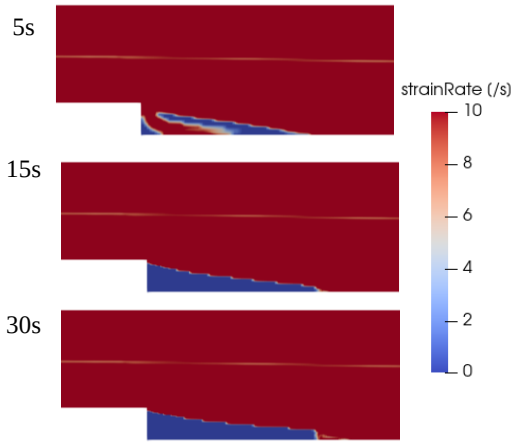

Figure 8. Fluid strain rate at t=5, 15 and 30s.

5. SUMMARY

This study proposes a thrombus formation model that integrates blood flow, platelet activity, and coagulation cascade to predict thrombus formation behavior in blood-contacting medical devices. The model was validated in a backward-facing step geometry, with its numerical simulation results achieving a high degree of consistency with experimental data. This research establishes a foundation for future studies and applications. By applying the proposed model to thrombus prediction in blood-contacting medical devices, it provides a scientific basis for optimizing device design, clinical treatments, and prognostic evaluations.

APPENDICES

Table A1. Parameter relate to platelets activity model

terms	expression	description
k_{apa}	$\begin{cases} 0, & \Omega < 1.0 \\ \frac{\Omega}{t_{ct}}, & \Omega \geq 1.0 \\ \frac{1}{t_{act}}, & \frac{\Omega}{t_{ct}} \geq \frac{1}{t_{act}} \end{cases}$	Platelet activation due to chemical agonists occurs only when the agonist concentration exceeds a certain threshold, triggering the chemical activation reaction.
Ω	$w_{ADP}\frac{[ADP]}{ADP_t}+w_{IIa}\frac{[IIa]}{IIa_t}$	The agonist equivalence, w_{ADP} and w_{IIa} , represent the specific weight factors of ADP and thrombin in their role in platelet activation.
k_{tb}	$k_{bb}\times f(\tau)$	The rate of thrombus breakdown[21]
k_{bb}	200	constant related to the thrombus breakdown rate[21]
$f(\tau)$	$\frac{\tau^2}{\tau^2+\tau_t^2}$	Switching function related to k_{tb}, the greater the scalar shear force acting on the thrombus unit, the faster the thrombus breakdown.
ϕ	$\frac{[BP]}{BP_t}$	Thrombus volume fraction. BPt=1×10^{12}PLT/m^3
λ_j	2.4×10^{-8}	The amount of ADP released by each activated platelet.

Table A2. Expressions of flux boundary conditions

species	expression	description
RP	$-S\theta k_{rpab}[RP]_{wall}$	Consumption due to RP directly adsorbing onto the foreign surface
AP	$S\theta k_{rpab}[RP]_{wall}$	Generated due to RP directly adsorbing onto the foreign surface
ADP	$\lambda_j S\theta k_{rpab}[RP]_{wall}$	ADP released by platelets during the conversion of RP to AP.
XII	$-k_1[XII]$	Consumption due to FXII directly adsorbing onto the foreign surface
XIIa	$k_1[XII]$	Generated due to FXII directly adsorbing onto the foreign surface

REFERENCES

[1] Nascimbene, A., Bark, D., and Smadja, D. M., 2023, "Hemocompatibility and Biophysical Interface of Left Ventricular Assist Devices and Total Artificial Hearts," Blood, Vol. 143, pp. 661–672.

[2] Manning, K. B., Nicoud, F., and Shea, S. M., 2021, "Mathematical and Computational Modeling of Device-Induced Thrombosis," Curr. Opin. Biomed. Eng., Vol. 20, p. 100349.

[3] Fogelson, A. L., 1992, "Continuum Models of Platelet Aggregation: Formulation and Mechanical Properties," SIAM J. Appl. Math., Vol. 52, pp. 1089–1110.

[4] 2008, "Immersed-Boundary-Type Models of Intravascular Platelet Aggregation," Comput. Methods Appl. Mech. Eng., Vol. 197, pp. 2087–2104.

[5] Sorensen, E. N., Burgreen, G. W., Wagner, W. R., and Antaki, J. F., 1999, "Computational Simulation of Platelet Deposition and Activation: I. Model Development and Properties," Ann. Biomed. Eng., Vol. 27, pp. 436–448.

[6] Goodman, P. D., Barlow, E. T., Crapo, P. M., Mohammad, S. F., and Solen, K. A., 2005,

"Computational Model of Device-Induced Thrombosis and Thromboembolism," Ann. Biomed. Eng., Vol. 33, pp. 780–797.
[7] Taylor, J. O., Meyer, R. S., Deutsch, S., and Manning, K. B., 2016, "Development of a Computational Model for Macroscopic Predictions of Device-Induced Thrombosis," Biomech. Model. Mechanobiol., Vol. 15, pp. 1713–1731.
[8] Wu, W.-T., Jamiolkowski, M. A., Wagner, W. R., Aubry, N., Massoudi, M., and Antaki, J. F., 2017, "Multi-Constituent Simulation of Thrombus Deposition," Sci. Rep., Vol. 7, p. 42720.
[9] Wu, W.-T., Yang, F., Wu, J., Aubry, N., Massoudi, M., and Antaki, J. F., 2016, "High Fidelity Computational Simulation of Thrombus Formation in Thoratec HeartMate II Continuous Flow Ventricular Assist Device," Sci. Rep., Vol. 6, p. 38025.
[10] Blum, C., Groß-Hardt, S., Steinseifer, U., and Neidlin, M., 2022, "An Accelerated Thrombosis Model for Computational Fluid Dynamics Simulations in Rotary Blood Pumps," Cardiovasc. Eng. Technol., Vol. 13, pp. 638–649.
[11] Li, Y., Wang, H., Fu, X., Xi, Y., Sun, A., Chen, Z., and Fan, Y., 2024, "A Comprehensive Study of Oxygenator Gas Transfer Efficiency and Thrombosis Risk," Phys. Fluids, Vol. 36, p. 081916.
[12] Li, Y., Wang, H., Liu, X., Xi, Y., Sun, A., Wang, L., Deng, X., Chen, Z., and Fan, Y., 2024, "Comprehensive Study on Simulation, Performance Evaluation and Optimization Strategies for Blood Pumps," Eng. Appl. Comput. Fluid Mech., Vol. 18, p. 2369690.
[13] Li, Y., Zhang, M., Sun, A., Wang, X., Fan, Y., and Chen, Z., 2024, "Evaluation and Optimization of Interventional Blood Pump Based on Hydraulic Performances and Hemocompatibility Performances," Phys. Fluids, Vol. 36, p. 111903.
[14] Méndez Rojano, R., Mendez, S., and Nicoud, F., 2018, "Introducing the Pro-Coagulant Contact System in the Numerical Assessment of Device-Related Thrombosis," Biomech. Model. Mechanobiol., Vol. 17, pp. 815–826.
[15] Méndez Rojano, R., Mendez, S., Lucor, D., Ranc, A., Giansily-Blaizot, M., Schved, J.-F., and Nicoud, F., 2019, "Kinetics of the Coagulation Cascade Including the Contact Activation System: Sensitivity Analysis and Model Reduction," Biomech. Model. Mechanobiol., Vol. 18, pp. 1139–1153.
[16] Anand, M., Rajagopal, K., and Rajagopal, K. R., 2003, "A Model Incorporating Some of the Mechanical and Biochemical Factors Underlying Clot Formation and Dissolution in Flowing Blood," J. Theor. Med., Vol. 5, pp. 183–218.
[17] Wang, Y., Luo, K., Qiao, Y., and Fan, J., 2021, "An Integrated Fluid-Chemical Model toward Modeling the Thrombus Formation in an Idealized Model of Aortic Dissection," Comput. Biol. Med., Vol. 136, p. 104709.
[18] Wang, Y., Luan, J., Luo, K., Zhu, T., and Fan, J., 2023, "Multi-Constituent Simulation of Thrombosis in Aortic Dissection," Int. J. Eng. Sci., Vol. 184, p. 103817.
[19] Yang, L., Neuberger, T., and Manning, K. B., 2021, "In Vitro Real-Time Magnetic Resonance Imaging for Quantification of Thrombosis," Magn. Reson. Mater. Phys. Biol. Med., Vol. 34, pp. 285–295.
[20] Menichini, C., and Xu, X. Y., 2016, "Mathematical Modeling of Thrombus Formation in Idealized Models of Aortic Dissection: Initial Findings and Potential Applications," J. Math. Biol., Vol. 73, pp. 1205–1226.
[21] Wang, K., Armour, C. H., Gibbs, R. G. J., and Xu, X. Y., 2023, "A Numerical Study of the Effect of Thrombus Breakdown on Predicted Thrombus Formation and Growth," Biomech. Model. Mechanobiol., Vol. 23, pp. 61–71.